Dalton Transactions

ROYAL SOCIETY OF CHEMISTRY

PAPER

View Article Online
View Journal | View Issue

Check for updates

Cite this: *Dalton Trans.*, 2024, **53**, 5702

Nitrate and nitroarene hydrogenations catalyzed by alkaline-earth nickel phosphide clathrates†

Marquix A. S. Adamson,[a] Lin Wei,[a] Philip Yox,[a,b] Fatema H. B. Hafiz[a] and Javier Vela *[a,b]

Received 2nd February 2024,
Accepted 20th February 2024

DOI: 10.1039/d4dt00332b

rsc.li/dalton

The alkaline-earth-containing nickel phosphide clathrates $AeNi_2P_4$ (Ae = Ba, Sr) are investigated as catalysts for the reduction of nitrate or nitroarenes in aqueous or ethanolic solution, respectively. While $AeNi_2P_4$ clathrates are inactive in their bulk polycrystalline form, they become active in nitrate hydrogenation after size reduction by either grinding or ball milling. However, while the clathrate structure remains intact after manual grinding, ball milling is of limited use as it results in significant clathrate degradation. Ground $AeNi_2P_4$ catalysts are also active in nitroarene hydrogenation. Condensation products such as azoxy- and azo-benzenes form early (4 h) but anilines accumulate after long reaction times (24 h). Unexpectedly, $BaNi_2P_4$ partially devinylates nitrostyrene to nitrobenzene. Overall, $BaNi_2P_4$ is more active than $SrNi_2P_4$ in both nitrate and nitroarene hydrogenation. These results showcase the potential utility of clathrates in a growing number of catalytic transformations.

Introduction

Green and sustainable chemistries benefit from catalysts that can efficiently remove pollutants or selectively generate value-added compounds.[1,2] For example, the reduction of nitrogen oxides and nitroarenes is key to addressing outstanding challenges posed by some of the multiple anthropogenic effects on the global nitrogen cycle as well as in the production of organic dyes for the fine chemicals and electronics industries. Specifically, high concentrations of nitrate (NO_3^-) in groundwater produced by the degradation of excess fertilizer has been linked to a higher incidence of cases of blue baby syndrome and certain forms of cancer.[3,4] Similarly, because of their mutagenicity or bioaccumulation, multiple nitroarenes including nitrobenzene are considered priority pollutants by the U.S. Environmental Protection Agency (EPA).[5–7] Therefore, new catalysts that can facilitate the removal of these contaminants by transforming them into less toxic and—ideally—more valuable products are highly desirable.

A potent method for reducing nitrate and nitroarenes to useful or relatively benign compounds is catalytic hydrogenation with H_2 or $NaBH_4$ (Scheme 1). Recent developments in this area include versatile bimetallic and intermetallic catalysts which,[8,9] in addition to reducing nitroarenes,[10–13] can in some cases tolerate a variety of functional groups.[14,15] Intermetallic nanocatalysts prepared from single-source heterobimetallic precursors have also exhibited a strong correlation between catalyst structure and product selectivity.[10,16,17] For example, depending on the crystalline phase of the nanocatalyst used, nitrobenzene is selectively reduced either directly to aniline or to azo(xy) condensation products formed by condensation of nitroso and hydroxylamine intermediates (Scheme 1b).[10,18]

In comparison to noble metal-containing catalysts, there are fewer base metal catalysts that permit the reduction of NO_3^- or nitroarenes at or near ambient conditions.[18–21] Among selected examples, we previously demonstrated that nanoscale Ni_2P catalyzes the full hydrogenation of NO_3^- with very high selectivity toward ammonia (NH_3).[22] Computations showed that the $Ni_2P(001)$ surface exhibits partial H• saturation coverage, which enables coadsorption and thus activation and reduction of NO_3^-. Interestingly, this led to the development of a self-sustainable photocatalytic NO_3^- reduction system using Ni_2P-modified, nanostructured semi-

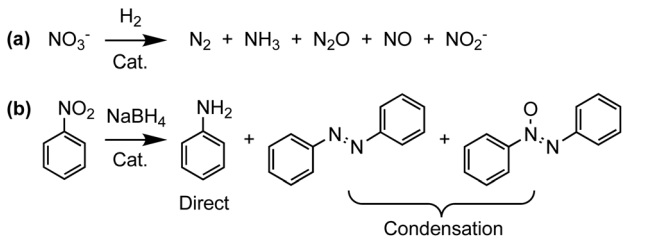

Scheme 1 Catalytic hydrogenations of nitrate and nitrobenzene showing some of their possible products.

[a]*Department of Chemistry, Iowa State University, Ames, Iowa 50011, USA. E-mail: vela@iastate.edu*
[b]*Ames National Laboratory, U.S. Department of Energy, Ames, Iowa 50011, USA*

†Electronic supplementary information (ESI) available: Hydrogenation results using different binary and ternary nickel phosphides, and powder XRD patterns of recovered clathrates. See DOI: https://doi.org/10.1039/d4dt00332b

conductors. Specifically, starting with 2 mM aqueous NO_3^-, heterostructured Ni_2P/Ta_3N_5 and Ni_2P/TaON displayed NO_3^- conversions as high as 79% and 61%, respectively, within 12 h under 419 nm light, which corresponded to apparent quantum yields of 3–4%.[23] Similar photocatalytic schemes have been reported for nitrobenzene.[24,25]

Because multiple first row, transition metal phosphides and related materials in addition to Ni_2P are also capable of catalyzing the hydrogen evolution reaction (HER)[26–28] as well as—its reverse—hydrogen activation, we wondered whether a more complex framework based on nickel phosphide could serve as a noble metal-free catalyst for nitrogen-centered hydrogenation. For example, transition metal-based clathrates exhibit high flexibility in their 3D frameworks. This prompted our interest in nickel phosphide clathrates such as $BaNi_2P_4$ and $SrNi_2P_4$, which are comprised of Ni_8P_{16} cages encapsulating alkaline-earth (Ae) guest atoms (Fig. 1).[29] Like Ni_2P and other transition metal phosphides, AM_2P_4 clathrates display metallic character, as determined through transport measurements and computations.[30] Moreover, the guest atom (Ba or Sr) affects the electron density and overall reactivity of the clathrate, which could open a new avenue for fine tuning the activity or selectivity of new families of catalysts.

In this work, we demonstrate that the ternary nickel phosphide clathrates $BaNi_2P_4$ and $SrNi_2P_4$ are indeed capable of catalyzing the hydrogenation of NO_3^- and nitroarenes at or near ambient temperature and atmospheric pressure. In the case of NO_3^- hydrogenation, $AeNi_2P_4$ clathrates are selective toward NH_3. Because this mimics the behavior of binary Ni_2P, we infer there may be mechanistic similarities between the two systems. We also find that, under the same conditions, $BaNi_2P_4$ achieves up to three times higher activity than $SrNi_2P_4$ in NO_3^- hydrogenation, which may be partly attributed to the exact nature of the guest atom. In the case of nitroarenes, these clathrates enable the formation of condensation products like azobenzene and azoxybenzene at early reaction times, although direct aniline products accumulate at longer times. From our previous work on nanoscale binary nickel phosphides, we believe that dimensional and electronic fine-tuning within the $AeNi_2P_4$ clathrate family and other similar frameworks may be used to further enhance their catalytic activity and selectivity.

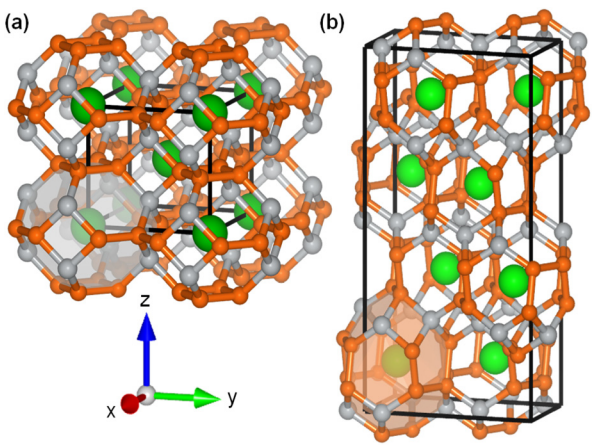

Fig. 1 Unit cells of the crystalline nickel phosphide clathrates (a) $BaNi_2P_4$ and (b) $SrNi_2P_4$ (green: Ba or Sr, grey: Ni, orange: P).[29,30]

Results and discussion

Catalyst dimensionality and activation

$AeNi_2P_4$ clathrates are typically made by a traditional, high-temperature, solid-state reaction where the elements are mixed, sealed in a silica ampule, and heated to 850 °C.[29] The resultant mixture is ground, resealed, and further annealed until phase-pure clathrates form, as determined by powder XRD (Fig. 2). As-prepared, polycrystalline or "bulk" $BaNi_2P_4$

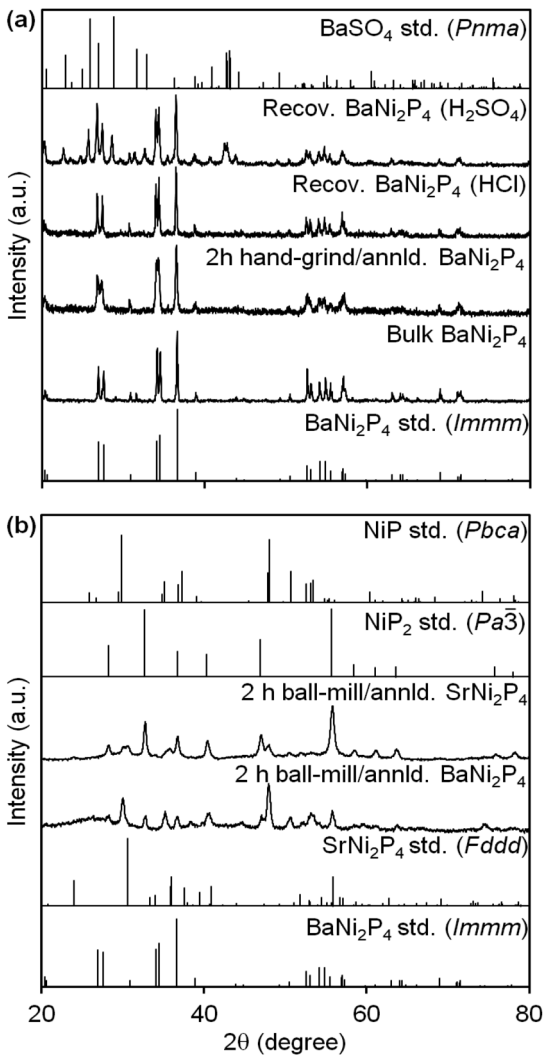

Fig. 2 Powder XRD of $AeNi_2P_4$ (Ae = Ba or Sr) clathrates before and after (a) hand-grinding or (b) ball-milling. XRD of two $BaNi_2P_4$ samples recovered after catalysis with different acids are included in (a). Reference XRD patterns are shown for comparison ($BaNi_2P_4$, ICSD79104; $SrNi_2P_4$, ICSD429359; NiP, ICSD27159; NiP_2, ICSD22221; $BaSO_4$, ICSD33730).

and $SrNi_2P_4$—with approximate particle sizes of 0.20–0.37 mm—are inactive toward NO_3^- hydrogenation (Table 1, entries 4 and 12). Previously, annealing under 1 atm of H_2 at 400 °C for 1 h was used to successfully activate nanocrystalline metal phosphides by removing capping ligands.[31] In addition, surface reconstruction induced by H• adsorption is known to enhance the activity of Ni_2P nanocatalysts.[22] Thus, even though the clathrates in this work lack surface ligands, we decided to follow a similar H_2 annealing and activation protocol across all of the different catalysts studied. Indeed, H_2 annealing partially activates bulk $BaNi_2P_4$ toward NO_3^- hydrogenation, achieving 10% reduction when starting from 2.0 mM aqueous NO_3^- at 60 °C and pH = 2 (using 10 mg catalyst, see Table 1 entry 5).

Smaller, nanoscale catalysts are known to have a much larger surface area and contain a higher concentration of active sites and defects that enhance catalytic performance.[32] In fact, nanocrystalline clathrates were recently prepared by ball milling or through ionic liquid-assisted approaches.[33,34] Therefore, we decided to explore whether a similar, top-down approach based on hand-grinding or ball-milling could be used to increase the surface area and, with it, enhance the catalytic activity of $AeNi_2P_4$ clathrates (Fig. 3).

Hand-grinding results in noticeable broadening of the reflections in the powder XRD of these materials, indicating a decrease in apparent particle size (Fig. 2a). Using the Scherrer equation, the average single crystalline domain size after 2 h of hand-grinding is as small as 44 ± 5 nm for $BaNi_2P_4$ and 40 ± 15 nm for $SrNi_2P_4$ (Table 1, entries 7 and 13). Scanning electron microscopy (SEM) images of the hand-ground clathrate powders confirm a substantial decrease in particle size—see ESI.†

In contrast to hand-grinding, ball-milling the clathrates for 2 h results in pronounced decay (Fig. 2b). After 2 h of ball-milling, $BaNi_2P_4$ completely decomposes into a mixture of nanocrystalline (<30 nm) NiP_2 (73%) and NiP (27%) (Table 1, entry 11). The strontium clathrate is only marginally more stable under these conditions: after 2 h of ball-milling, 29% of nanocrystalline $SrNi_2P_4$ remains (9.6 ± 2.1 nm; Table 1, entry 15). Thus, while both hand-grinding and ball-milling are effective at decreasing particle size, only the former can keep the clathrate phase intact.

Particle size, binary comparison, and effect of guest atom

Because the localized high pressure and excessive shear produced by ball-milling results in significant clathrate decomposition, we focused on hand-grinding for a majority of the catalysis experiments in this study. Fig. 3a shows that there is a fairly linear relationship between NO_3^- conversion with $BaNi_2P_4$ and the length of time the material is hand-ground prior to catalysis. With the aforementioned standard conditions—2.0 mM aq. NO_3^- at 60 °C, pH = 2, 10 mg catalyst—conversion reaches 25% and 79% after 0.5 h and 2 h of hand-grinding, respectively (Table 1, entries 5–7). Fig. 3b further demonstrates the effect that grinding has in decreasing average particle size and increasing NO_3^- conversion. Interestingly, while ball-milling for 0.5 h also results in a modest 30% conversion, this effect tapers off after ball-milling for 2 h, which results in only 43% conversion (about half of the maximum overall activity observed after hand-grinding the catalyst; entries 7–11). In addition, the activity of the latter likely stems from the presence of nickel phosphide binaries produced by the decomposition of the clathrate under ball milling conditions.

Based on their turnover numbers (TONs) and turnover frequencies (TOFs), the clathrate catalysts used here have comparable or superior activity relative to the better-known nanoscale binary nickel phosphides Ni_5P_4 and Ni_2P (Table 1, entries 2–3, 7).[22] The clathrates are also highly selective to ammonium (NH_4^+; produced by protonation of NH_3 under the acidic conditions used). For example, under the same conditions above, nanocrystalline Ni_2P and Ni_5P_4 reduce 98% and 81% of NO_3^- within 4 h (Fig. 3c). In comparison, hand-ground $BaNi_2P_4$ only reaches similar NO_3^- conversion and NH_4^+ selectivity after 12 h (entry 7). As in the case of the bulk clathrates above, bulk Ni_2P and Ni_5P_4 are also inactive. Therefore, clear opportunities exist to further control the dimensionality and, with it, the activity of $AeNi_2P_4$ clathrate nanocatalysts.

Multiple factors inherent to the catalyst may contribute to differences in catalytic performance, such as the electronegativities and ionic sizes of the guest atoms, and the size and shape of the clathrate cages. The electronegativity of the guest atom—0.89 for Ba and 0.95 for Sr—may affect the electron density on the catalyst surface,[35] consequently influencing the ability to bind and activate NO_3^- and H_2. Similarly, the different nickel phosphide frameworks may show different nitrate and hydrogen adsorption energetics. The larger, truncated octahedral cages encapsulate Ba^{2+} (156 pm ionic radius) cations, whereas the smaller, twisted Kelvin cells encapsulate Sr^{2+} (140 pm) cations.[36] As measured by the TON and TOF values achieved by each catalyst, hand-ground $BaNi_2P_4$ (1188, 99 h^{-1}) outperforms hand-ground $SrNi_2P_4$ (324, 27 h^{-1}) in our NO_3^- hydrogenation experiments (Table 1). This suggests that more electropositive metals and larger cages could enhance the clathrate's nitrate reduction ability.

Acid effect and identity of recovered catalysts

Similar to the hydrogen evolution reaction (HER),[22,23,37] NO_3^- hydrogenation with metal phosphides is pH dependent, becoming faster with the increased acidity of the medium. In the case of the clathrates here, initial acidification with H_2SO_4, HNO_3, or HCl has some impact in catalytic behavior. More specifically, NO_3^- conversions range depending on the acid and catalyst combination used (see below). For example, there is a drastic rise in conversion over hand-ground $BaNi_2P_4$ from 6.5% to 79% in going from HCl to HNO_3 to H_2SO_4 (Table 1, entries 7–9). In most cases, at least 25% of the initial NO_3^- is reduced within 12 h at 60 °C and pH = 2, and always with a high selectivity for NH_4^+ (2.0 mM initial aq. NO_3^-, 10 mg of catalyst; see ESI†).

To further probe the reasons behind these differences, we recovered the solids left after select catalytic experiments and

Table 1 Nitrate and nitroarene reductions using nickel phosphide and clathrate catalysts

	Catalyst	Pretreatment[a]	Pretreated XRD (nm)[b]	Reactant[c]	*t* (h)	Conversion (%)	Product(s) (selec./%)	Recovered XRD (nm)[b]	TON[d] (TOF[e] h^{-1})
1	None	—	—	NO_3^-	12	0	—	—	—
2	Ni_2P[g]	Annld.[f]		NO_3^-	4	98	NH_4^+ (100)	—	31 (8)
3	Ni_5P_4[g]	Annld.[f]		NO_3^-	4	81	NH_4^+ (100)	—	1149 (287)
4	$BaNi_2P_4$[g]	—	$BaNi_2P_4$ (0.2 mm)	NO_3^-	12	0	—	—	—
5	$BaNi_2P_4$[g]	Annld.[f]	$BaNi_2P_4$ (0.2 mm)	NO_3^-	12	10	NH_4^+ (100)	—	—
6	$BaNi_2P_4$[g]	h/2 Hand-grind, annld.[f]	$BaNi_2P_4$ (0.35 μm)	NO_3^-	12	25	NH_4^+ (100)	—	—
7	$BaNi_2P_4$[g]	2 h Hand-grind, annld.[f]	$BaNi_2P_4$ (44 ± 5)	NO_3^-	12	79	NH_4^+ (94)	65% $BaNi_2P_4$ (59 ± 15), 35% $BaSO_4$ (40 ± 3)	1188 (99)
8	$BaNi_2P_4$[h]	2 h Hand-grind, annld.[f]	$BaNi_2P_4$ (44 ± 5)	NO_3^-	12	15	NH_4^+ (100)	69% $BaNi_2P_4$ (44 ± 13), 31% Ni_2P (32 ± 9)	—
9	$BaNi_2P_4$[i]	2 h Hand-grind, annld.[f]	$BaNi_2P_4$ (44 ± 5)	NO_3^-	12	6.5	NH_4^+ (100)	$BaNi_2P_4$ (82 ± 10)	—
10	$BaNi_2P_4$[g]	h/2 Ball-mill, annld.[f]	73% NiP_2 (52 ± 39), 27% ZrO_2? (>100).	NO_3^-	12	30	NH_4^+ (100)		—
11	$BaNi_2P_4$[g]	2 h Ball-mill, annld.[f]	73% NiP (20 ± 6), 27% NiP_2 (27 ± 1)	NO_3^-	12	43	NH_4^+ (100)	50% $BaSO_4$ (55 ± 33), 37% NiP_2 (38 ± 27), 13% ZrO_2? (>100)	—
12	$SrNi_2P_4$[g]	—	$SrNi_2P_4$ (0.37 mm)	NO_3^-	6	0	—	—	—
13	$SrNi_2P_4$[g]	2 h Hand-grind, annld.[f]	$SrNi_2P_4$ (40 ± 15)	NO_3^-	12	28	NH_4^+ (91)	$SrNi_2P_4$ (51 ± 1)	324 (27)
14	$SrNi_2P_4$[h]	2 h Hand-grind, annld.[f]	$SrNi_2P_4$ (40 ± 15)	NO_3^-	12	50	NH_4^+ (100)	62% $SrNi_2P_4$ (63 ± 3), 38% Ni_2P (32 ± 6)	—
15	$SrNi_2P_4$	2 h Ball-mill, annld.[f]	29% $SrNi_2P_4$ (9.6 ± 2.1), 51% NiP_2 (16 ± 6), 20% NiP (14 ± 4)	—	—	—	—		—
16	None	—	—	$PhNO_2$	4	9	—	—	—
17	$BaNi_2P_4$	2 h Hand-grind, annld.[f]		$PhNO_2$	4	47	Aniline (4), azo (7), azoxy (89)	—	—
18	$BaNi_2P_4$	2 h Hand-grind, annld.[f]		$PhNO_2$	24	98	Aniline (48), azo (49), azoxy (3)	—	2456 (102)
19	$SrNi_2P_4$	2 h Hand-grind, annld.[f]		$PhNO_2$	4	45	Aniline (4), azo (2), azoxy (94)	—	—
20	$SrNi_2P_4$	2 h Hand-grind, annld.[f]		$PhNO_2$	24	58	Aniline (16), azo (19), azoxy (65)	—	1114 (46)
21	$BaNi_2P_4$	2 h Hand-grind, annld.[f]		3-Nitrostyrene	4	95	Aniline[j] (16), azo[j] (8), azoxy[j] (69), devinyl.[k] (1), ethyl[j] (26)	—	—
22	$BaNi_2P_4$	2 h Hand-grind, annld.[f]		3-Nitrostyrene	24	99	Aniline[j] (20), azo[j] (0), azoxy[j] (54), devinyl. (39)[k], ethyl[j] (38)	—	2481 (103)

[a] 10 mg cat. [b] Estimated from XRD peak widths using the Scherrer equation when <100 nm; reported in nm unless specified otherwise. [c] 2.0 mM NO_3^- or NO_2^-, 60 °C, pH = 2/H_2O; or 50 mM nitroarene, RT/EtOH. [d] TON = moles of converted reactant/moles of surface-active catalyst sites (calculated for select cases, only). [e] TOF = TON/catalysis time. [f] 1 atm H_2, 1 h, 400 °C. Adjusted pH with: [g] H_2SO_4, [h] HNO_3, or [i] HCl. [j] Products with functional group (see ESI†). [k] Multiple Ph–vinyl (C–C) breaking products.

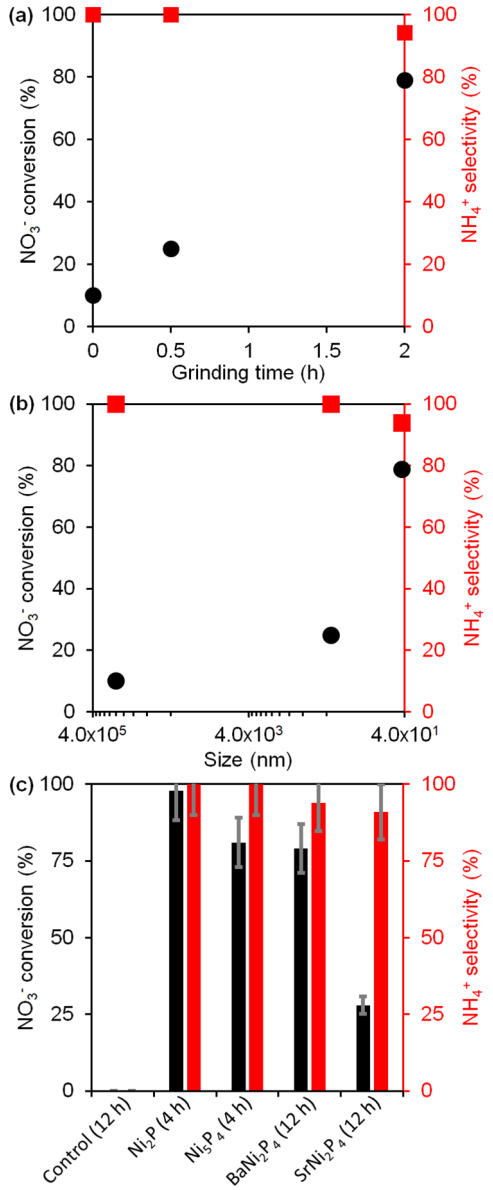

Fig. 3 Catalytic activity (●) and selectivity (■) of $BaNi_2P_4$ against NO_3^- hydrogenation as a function of (a) hand-grinding time (prior to catalysis) and (b) particle size (12 h reaction data shown). (c) Catalytic activity (black) and selectivity (red) of nanocrystalline binary phosphides *vs.* 2 h hand-ground clathrates (Table 1, entries 1–3, 7 and 13). (General conditions: 2 mM aqueous NO_3^-, 60 °C, pH = 2—adjusted with H_2SO_4—see Experimental).

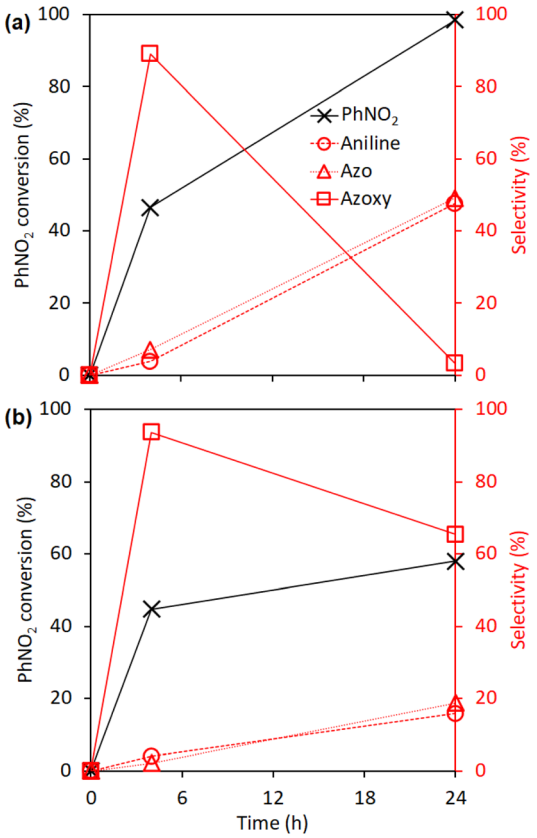

Fig. 4 Catalytic activity (black) and selectivity (red) of (a) $BaNi_2P_4$ and (b) $SrNi_2P_4$ against nitrobenzene reduction. (Conditions: 50 mM $PhNO_2$, R.T.; catalysts hand-ground for 2 h and annealed under H_2—see Experimental).

re-measured their powder XRD. As shown in Fig. 2, $BaNi_2P_4$ is unaffected when HCl is used, and the catalyst retains the same crystalline phase without any byproducts or impurities (Table 1, entry 9, see ESI†). In contrast, changing the proton source to H_2SO_4 leads to the formation of a small amount of insoluble $BaSO_4$; however, a majority of the recovered solids are still made of crystalline $BaNi_2P_4$ (Table 1, entries 7). Across all experiments, there is a slight decrease in the Scherrer size of the clathrates after catalysis, suggesting that some catalyst etching and dissolution occur.

Nitroarene reduction and chemoselectivity

We next turned our attention to the ability of the clathrates to mediate the reduction of nitroarenes in ethanol (Scheme 1b). Previous reports showed that nickel phosphide nanoparticles —like Ni_2P and $Ni_{12}P_5$—are highly active catalysts for reducing nitrobenzene,[38] benzonitrile,[39] and other nitroarenes.[40,41] The reduction of nitroarenes normally occurs with high selectivity for the direct aniline products over a period of a few hours.

Benchtop hydrogenation of nitrobenzene is catalyzed by the hand-ground clathrates $BaNi_2P_4$ and $SrNi_2P_4$ (Fig. 4). $BaNi_2P_4$ fully reduces nitrobenzene within 24 h under ambient conditions—when starting with 50 mM nitroarene and using 10 mg of catalyst (see Experimental). However, unlike regular nitroarene reduction, quantification by GCMS shows clathrate catalysis follows an indirect pathway to aniline by means of forming condensation products like azobenzene and azoxybenzene at first (Table 1, entry 18). The condensation pathway is similarly followed when using $SrNi_2P_4$, yet less than 60% of the starting material is converted within the same timeframe under the same conditions (Table 1, entry 20). As a direct comparison between catalysts, $BaNi_2P_4$ reaches TON and TOF values of 2456 and 102 h^{-1}, respectively, while $SrNi_2P_4$ is *ca.* half as active, with TON and TOF values of 1114 and 46 h^{-1},

respectively. These results are consistent with the NO_3^- hydrogenation experiments discussed above, where the barium clathrate is also the more active catalyst. In other words, the sterically bulkier nitrobenzene molecules are more rapidly reduced over catalysts containing the more electropositive metal (Ba) and the larger cage clathrate ($BaNi_2P_4$).

We further probed the activity and chemoselectivity of the activated $AeNi_2P_4$ clathrates against 3-nitrostyrene, containing both nitro and vinyl groups, both of which are susceptible to chemical reduction (Scheme 2). Nitrostyrene is a reactant often employed in catalytic reductions to study the chemoselectivity against different functional groups.[42–44] Under ambient conditions and starting with 50 mM of 3-nitrostyrene and using 10 mg catalyst, both $BaNi_2P_4$ and $SrNi_2P_4$ show 95% conversion—TONs and TOFs of 2481–1882 and 103–78 h^{-1}—within 4 h (Fig. 5; Table 1, entry 21, see Experimental). Interestingly, the clathrate catalysts consistently show a strong preference for the activation of nitro over vinyl groups, with marked selectivity for azo(xy) condensation products over anilines, ethyl benzenes, or other reduction products.

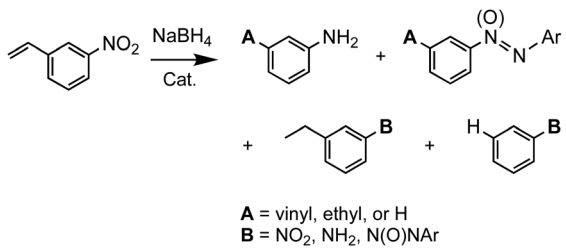

Scheme 2 Catalytic hydrogenation of 3-nitrostyrene showing some of its possible products.

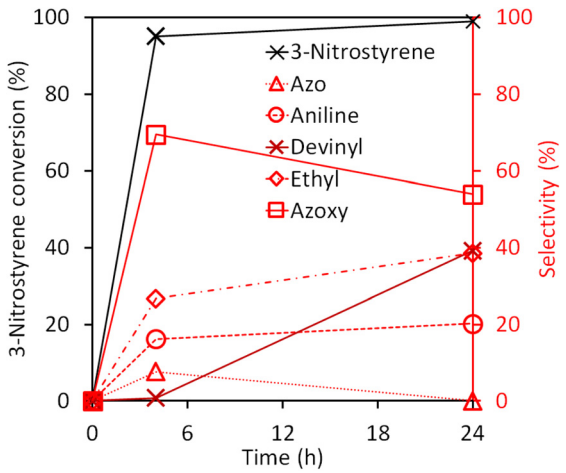

Fig. 5 Catalytic activity (black) and selectivity (red) of $BaNi_2P_4$ against 3-nitrobenzene hydrogenation. (Conditions: 50 mM 3-NO_2-styrene, R.T.; catalyst hand-ground for 2 h and annealed under H_2, see Experimental and ESI†).

Unexpected devinylation and surface analysis

Interestingly, catalytic runs over 24 h using hand-ground $BaNi_2P_4$ result in a substantial amount of a different and unexpected product, nitrobenzene (Table 1, entry 22). Unlike ethyl reduction products formed by the selective reduction of the styrene double bond, devinylated products like nitrobenzene are formed by the activation and reduction of the aromatic (Ar) C–aliphatic(C) bond in 3-nitrostyrene, leading to loss of the vinyl group. Notably, devinylation is specific to the more active $BaNi_2P_4$ clathrate after hand grinding and H_2-annealing and is absent with the other catalysts tested. After 24 h with this catalyst, devinylated aromatics are the second-most prominent class of reduction products behind azo(xy) compounds.

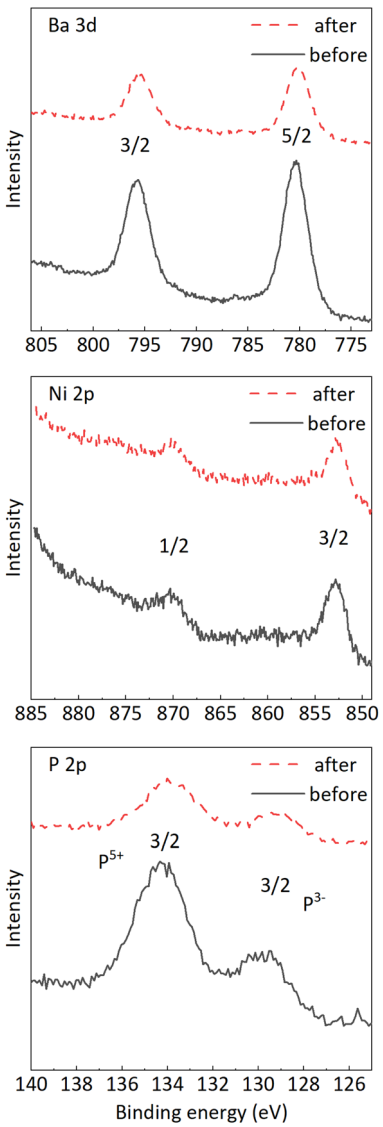

Fig. 6 Ba 3d, Ni 2p, and P 2p XPS regions of $BaNi_2P_4$ before (black) and after (red) catalytic hydrogenation of 3-nitrostyrene. (Conditions: 50 mM 3-NO_2-styrene, R.T.; catalyst hand-ground for 2 h and annealed under H_2, see Experimental and ESI†).

To our knowledge, this represents one of the first reports of barium- or clathrate-based devinylation of a styrene. Previous examples of styrene devinylation and related carbon–carbon bond activation require similarly long reaction times (12–24 h) but significantly higher temperatures (80–180 °C)—whereas this work takes place at ambient temperature.[45,46] Similar to our results, reported styrene devinylation yields remain moderate (<50%).[47] Additional investigations are ongoing to probe the nature of the active species, the reaction mechanism, and possible optimization of this unique, clathrate-mediated transformation.

Finally, because surface chemistry plays a key role in determining catalytic activity, we studied one of the clathrates at different stages of catalysis by X-ray photoelectron spectroscopy (XPS) (Fig. 6). Specifically, we find that the spectra of $BaNi_2P_4$ before and after the hydrogenation of 3-nitrostyrene show XPS peaks corresponding to Ba, Ni, and P species (in addition to C and O, see ESI†). In all samples, the Ba $3d_{5/2}$ region shows two main peaks at 780.3 eV and 795.6 eV, which can be attributed to Ba^{2+}.[48] Also, the Ni $2p_{3/2}$ and Ni $2p_{1/2}$ regions exhibit peaks at 852.6 eV and 870.3 eV, which are reminiscent of the low valent '$Ni^{\delta+}$' sites present in Ni_2P;[22] however, unlike the XPS of Ni_2P, the Ni region in $BaNi_2P_4$ lacks a Ni^{2+} impurity.[22] In all cases, the P 2p region contains two peaks: a more prominent peak at a binding energy of 134.3 eV, corresponding to the oxidized form P^{5+}—surface PO_4^{3-} impurity—and a smaller peak at 129.1 eV corresponding to P^{3-}—phosphide. Because the XPS spectra lack any evidence of other species that could be catalytically active, such as Ni^{2+} or Ni^0, and because the XPS spectra are equivalent before and after catalysis, we conclude that the active species under an atmosphere of H_2 exists on the surface of the clathrate crystals.

Conclusions

In summary, top-down approaches to reducing the particle size of bulk nickel phosphide clathrates $AeNi_2P_4$ (A = Ba, Sr) such as hand-grinding or ball-milling, followed by thermal annealing under H_2 results in their activation toward the hydrogenation of aqueous NO_3^- or the reduction of nitroarenes. While ball milling is a well-known technique for conveniently reducing particle size, our studies show that ball milling leads to significant degradation of the clathrate phases into binary phosphides. This underscores how careful characterization of the catalyst after activation as well as before and after catalysis is key to identifying the actual active species. Fortunately, hand grinding is a milder way to decrease particle size and increase the surface area and catalytic activity, while at the same time preserving the integrity of the clathrate phase.

Without size reduction, the bulk clathrates lack catalytic activity. After hand-grinding and H_2 annealing, $BaNi_2P_4$ converts 79% NO_3^- under near-ambient conditions (10 mg catalyst, 1 atm H_2, 60 °C, pH = 2, 12 h) starting from 2.0 mM NO_3^- and is highly selective toward NH_4^+. Longer hand-grinding times result in higher NO_3^- conversions in a nearly linear fashion. We also observe that lowering the pH of the initial solution with different acids can have a direct impact on the overall efficiency of the catalysis. In all cases, turnover number and frequency calculations show that the $BaNi_2P_4$ clathrate is the more active catalyst against both NO_3^- and nitrobenzene reduction. $BaNi_2P_4$ fully reduces nitrobenzene and nitrostyrene within 24 h under ambient conditions using 10 mg catalyst and 50 mM nitroarene. Within the same timeframe and under the same conditions, $SrNi_2P_4$ partially reduces nitrobenzene and fully reduces nitrostyrene. Interestingly, a previously unreported devinylation of nitrostyrene to nitrobenzene occurs when using the more active $BaNi_2P_4$ clathrate catalyst. Grinding appears to have an immense effect on the ability of the catalyst to devinylate, as this reaction is absent when bulk $BaNi_2P_4$ is used.

Given that a small particle size and high surface area are key to successful catalytic reduction with $AeNi_2P_4$ clathrates, additional synthesis of nanosized $AeNi_2P_4$ and similar phases may enable additional catalytic studies and applications. Furthermore, other nickel phosphide clathrates containing one or more guest atoms (*e.g.*, $EuNi_2P_4$) may be used to further enhance or fine tune the catalytic activity and selectivity of nitrogen-based and similar reductions.

Experimental

Materials

Metallic barium (Ba, 99.9%), strontium (Sr, 99.9%), copper powder (Cu, 99.9%), and 3-nitrostyrene (96%) were purchased from Sigma-Aldrich; nitrobenzene (99%) from Oakwood Chemical; sodium borohydride ($NaBH_4$, 99%) from Acros Organics; ethanol (EtOH, 200 proof) from Decon Labs; nickel powder (Ni, 99.996%) and red phosphorus (P_4, 99%) from Alfa Aesar; sulfuric acid (H_2SO_4, certified ACS plus), hydrochloric acid (HCl, certified ACS plus), nitric acid (HNO_3, certified ACS plus), and sodium nitrate ($NaNO_3$, certified ACS) from Fisher; hydrogen gas (H_2) and argon gas (Ar) from Airgas. Colorimetric kits (0.10–25.0 mg L^{-1} NO_3–N, 0.002–1.00 mg L^{-1} NO_2–N, 2.0–150 mg L^{-1} NH_4–N) were purchased from Merck. All chemicals were used as received. MilliQ water was used over all experiments.

Sample preparation

We prepared nanostructured Ni_2P and Ni_5P_4 using previously reported methods. In all cases, annealing under 1 atm of H_2 at 400 °C for 1 h was performed before catalysis.[22,49] Nickel phosphide clathrates $AeNi_2P_4$ (Ae = Ba, Sr) were synthesized as previously reported.[29,30] $BaNi_2P_4$ and $SrNi_2P_4$ were synthesized by stoichiometric solid-state reactions between the elements in glassy carbon crucibles sealed in evacuated silica ampules. Samples were heated to 850 °C over a period of 17 h, and then kept at this temperature for 140 h. Samples were opened in an Ar glovebox, ground, resealed, and reannealed in a similar manner. This grind-seal-anneal process was repeated 2–3

times until phase-pure samples were obtained. As prepared clathrates were ground in an agate mortar for 0.5–2 h, then annealed under 1 atm H_2 (5–10% H_2 in Ar) at 400 °C for 1 h.

Characterization

UV–Vis absorption spectra were collected with a photodiode-array Agilent 8453 UV–Vis spectrometer. Powder X-ray diffraction (XRD) was recorded using a Rigaku Ultima IV diffractometer with a Cu Kα radiation (40 kV, 44 mA). X-ray photoelectron spectroscopy (XPS) was conducted with a Kratos Amicus/ESCA 3400 instrument. The samples were irradiated with 240 W unmonochromated Mg Kα X-rays, and photoelectrons emitted at 0° from the surface were energy analyzed using a DuPont type analyzer. The pass energy was set at 150 eV. CasaXPS was used to process the raw data files. The binding energy of C 1s at 284.8 eV was used for reference.

NO_3^- catalytic hydrogenation

Approximately 10 mg of dry catalyst was placed in an H_2-filled 3-neck round bottom flask. 30 mL of an aqueous solution of $NaNO_3$ or HNO_3 (2.0 mM), previously sparged with Ar for 15–20 min was added to the flask and the pH was adjusted with H_2SO_4 or HCl. 1 atm of H_2 (5–10% in Ar) was introduced into the reactor at a rate of 20 mL min^{-1} while vigorously stirring at 700 RPM at 60 °C. Aliquots were taken at different times for colorimetric quantification of the different aqueous NO_3^-, NO_2^- and NH_4^+ products.

Nitroarene catalysis

Nitrobenzene (0.1 mmol, 10 μL) or 3-nitrostyrene (0.1 mmol, 14 μL) and ethanol (2 mL) were placed in a 5 mL vial. After stirring to ensure homogeneity, an aliquot was taken out, diluted, and analyzed by GCMS. 10 mg of a ground and annealed clathrate sample was then added and stirred at 300 RPM, followed by $NaBH_4$ (23 mg, 0.6 mmol) while stirring continued. Aliquots were taken at certain times and filtered using 0.2 μm PTFE syringe filters. Part of the filtered aliquots were then diluted for use in GCMS analysis.

Conflicts of interest

There are no conflicts to declare.

Acknowledgements

We thank the U.S. National Science Foundation, Division of Chemistry, Macromolecular, Supramolecular, and Nanochemistry Program (2305062) for funding of this work. We thank Dapeng Jing for assistance with XPS spectroscopy.

References

1 J. Wang, W. S. Cheon, J.-Y. Lee, W. Yan, S. Jung, H. W. Jang and M. Shokouhimehr, *Dalton Trans.*, 2023, **52**, 3567–3574.
2 R. Rameshan, A. Tiwari, S. Kanungo and S. Roy, *Inorg. Chem.*, 2023, **62**, 9934–9944.
3 A. J. Burgin and S. K. Hamilton, *Front. Ecol. Environ.*, 2007, **5**, 89–96.
4 S. Seitzinger, J. A. Harrison, J. K. Böhlke, A. F. Bouwman, R. Lowrance, B. Peterson, C. Tobias and G. Van Drecht, *Ecol. Appl.*, 2006, **16**, 2064–2090.
5 United States Environmental Protection Agency. *Priority Pollutant List*, 2014. **https://www.epa.gov/sites/default/files/2015-09/documents/priority-pollutant-list-epa.pdf** (Accessed 2023-1-8).
6 M. Bilal, A. R. Bagheri, P. Bhatt and S. J. Chen, *J. Environ. Manage.*, 2021, **291**, 112685-1–112685-13.
7 J. Tiwari, P. Tarale, S. Sivanesan and A. Bafana, *Environ. Sci. Pollut. Res.*, 2019, **26**, 28650–28667.
8 I. Sanchis, E. Diaz, A. H. Pizarro, J. J. Rodriguez and A. F. Mohedano, *Sep. Purif. Technol.*, 2022, **290**, 120750-1–120750-10.
9 M. Armbrüster, *Sci. Technol. Adv. Mater.*, 2020, **21**, 303–322.
10 C. L. Daniels, D.-J. Liu, M. A. S. Adamson, M. Knobeloch and J. Vela, *J. Phys. Chem. C*, 2021, **125**, 24440–24450.
11 S. Guo, H. Li, K. N. Heck, X. Luan, W. Guo, G. Henkelman and M. S. Wong, *Appl. Catal., B*, 2022, **305**, 121048-1–121048-9.
12 Z. Shen, G. Peng, Y. Gao and J. Shi, *Environ. Sci.: Water Res. Technol.*, 2021, **7**, 1078–1089.
13 M. Gholinejad, F. Khosravi, M. Afrasi, J. M. Sansano and C. Nájera, *Catal. Sci. Technol.*, 2021, **11**, 2652–2702.
14 M. Chen, C. R. Bowers and W. Huang, *Acc. Mater. Res.*, 2021, **2**, 1190–1202.
15 L. Zhang, J. Pan, L. Liu, S. Zhang, X. Wang, S. Song and H. Zhang, *Small*, 2022, 2201271-1–2201271-6.
16 C. L. Daniels, D. L. Mendivelso-Perez, B. A. Rosales, D. You, S. Sahu, J. S. Jones, E. A. Smith, F. P. Gabbaï and J. Vela, *ACS Omega*, 2019, **4**, 5197–5203.
17 C. L. Daniels, M. Knobeloch, P. Yox, M. A. S. Adamson, Y. Chen, R. W. Dorn, H. Wu, G. Zhou, H. Fan, A. Rossini and J. Vela, *Organometallics*, 2020, **39**, 1092–1104.
18 M. A. S. Adamson, P. Yox, T. Hernandez, F. Wang and J. Vela, *Chem. Mater.*, 2022, **34**, 746–755.
19 Y. Sheng, X. Lin, S. Yue, Y. Liu, X. Zou, X. Wang and X. Lu, *Mater. Adv.*, 2021, **2**, 6722–6730.
20 A. L. Schio, M. R. F. Soares, G. Machado and T. Barcellos, *ACS Sustainable Chem. Eng.*, 2021, **9**, 9661–9670.
21 D.-Y. Kuo, E. Nishiwaki, R. A. Rivera-Maldonado and B. M. Cossairt, *ACS Catal.*, 2023, **13**, 287–295.
22 L. Wei, D.-J. Liu, B. A. Rosales, J. W. Evans and J. Vela, *ACS Catal.*, 2020, **10**, 3618–3628.
23 L. Wei, M. A. S. Adamson and J. Vela, *ChemNanoMat*, 2020, **6**, 1179–1185.
24 Y. Dai, C. Li, Y. Shen, T. Lim, J. Xu, Y. Li, H. Niemantsverdriet, F. Besenbacher, N. Lock and R. Su, *Nat. Commun.*, 2018, **9**, 60.
25 L. Pei, H. Tan, M. Liu, R. Wang, X. Gu, X. Ke, J. Jia and Z. Zheng, *Green Chem.*, 2021, **23**, 3612–3622.

26 J. F. Callejas, C. G. Read, C. W. Roske, N. S. Lewis and R. E. Schaak, *Chem. Mater.*, 2016, **28**, 6017–6044.
27 A. T. Landers, M. Fields, D. A. Torelli, J. Xiao, T. R. Hellstern, S. A. Francis, C. Tsai, J. Kibsgaard, N. S. Lewis, K. Chan, C. Hahn and T. F. Jaramillo, *ACS Energy Lett.*, 2018, **3**, 1450–1457.
28 M. F. Delley, Z. Wu, M. E. Mundy, D. Ung, B. M. Cossairt, H. Wang and J. M. Mayer, *J. Am. Chem. Soc.*, 2019, **141**, 15390–15402.
29 J.-A. Dolyniuk, J. Wang, K. Lee and K. Kovnir, *Chem. Mater.*, 2015, **27**, 4476–4484.
30 J. Wang, J.-A. Dolyniuk, E. H. Krenkel, J. L. Niedziela, M. A. Tanatar, E. I. Timmons, T. Lanigan-Atkins, H. Zhou, Y. Cheng, A. J. Ramirez-Cuesta, D. L. Schlagel, U. S. Kaluarachchi, L.-L. Wang, S. L. Bud'ko, P. C. Canfield, R. Prozorov, O. Delaire and K. Kovnir, *Chem. Mater.*, 2020, **32**, 7932–7940.
31 E. J. Popczun, J. R. McKone, C. G. Read, A. J. Biacchi, A. M. Wiltrout, N. S. Lewis and R. E. Schaak, *J. Am. Chem. Soc.*, 2013, **135**, 9267–9270.
32 C. Xie, D. Yan, H. Li, S. Du, W. Chen, Y. Wang, Y. Zou, R. Chen and S. Wang, *ACS Catal.*, 2020, **10**, 11082–11098.
33 R. Shirataki, M. Hokazono, T. Nakabayashi and H. Anno, *IOP Conf. Ser.: Mater. Sci. Eng.*, 2011, **18**, 142012.
34 P. Simon, Z. Tang, W. Carrillo-Cabrera, K. Chiong, B. Böhme, M. Baitinger, H. Lichte, Y. Grin and A. M. Guloy, *J. Am. Chem. Soc.*, 2011, **133**, 7596–7601.
35 J. Mullay, *Estimation of Atomic and Group Electronegativities. In Structure and Bonding*, ed. K. D. Sen and C. K. Jørgensen, Springer, Berlin, Heidelberg, 1987, pp 1–25.
36 J.-A. Dolyniuk, B. Owens-Baird, J. Wang, J. V. Zaikina and K. Kovnir, *Mater. Sci. Eng.*, 2016, **108**, 1–46.
37 J. F. Callejas, J. M. McEnaney, C. G. Read, J. C. Crompton, A. J. Biacchi, E. J. Popczun, T. R. Gordon, N. S. Lewis and R. E. Schaak, *ACS Nano*, 2014, **8**, 11101–11107.
38 P. Liu, Z.-X. Zhang, S. W. Jun, Y.-L. Zhu and Y.-X. Li, *React. Kinet. Mech. Catal.*, 2019, **126**, 453–461.
39 Y.-F. Zen, Z.-C. Fu, F. Liang, Y. Xu, D.-D. Yang, Z. Yang, X. Gan, Z.-S. Lin, Y. Chen and W.-F. Fu, *Asian J. Org. Chem.*, 2017, **6**, 1589–1593.
40 T. Geng, H. Wang, H. Wu and S. Zhang, *J. Nanopart. Res.*, 2020, **22**, 237.
41 R. Gao, L. Pan, W. Wang, X. Zhang, L. Wang and J. J. Zou, *ACS Catal.*, 2018, **8**, 8420–8429.
42 L. Zhang, M. Zhou, A. Wang and T. Zhang, *Chem. Rev.*, 2020, **120**, 683–733.
43 Y. Pei, Z. Qi, T. W. Goh, L.-L. Wang, R. V. Maligal-Ganesh, H. L. MacMurdo, S. Zhang, C. Xiao, X. Li, F. F. Tao, D. D. Johnson and W. Huang, *J. Catal.*, 2017, **356**, 307–314.
44 S. Furukawa, Y. Yoshida and T. Komatsu, *ACS Catal.*, 2014, **4**, 1441–1450.
45 S. B. Bharate, R. Mudududdla, R. Sharma and R. A. Vishwakarma, *Tetrahedron Lett.*, 2013, **54**, 2913–2915.
46 R. K. DiNello and D. H. Dolphin, *J. Org. Chem.*, 1981, **46**, 3498–3502.
47 T. Hisayasu, N. Hara and H. Tamiaki, *Bull. Chem. Soc. Jpn.*, 2022, **95**, 1553–1560.
48 The international XPS database for XPS reference spectra. (**https://xpsdatabase.net/**). (Accessed 2023-11-16).
49 K. Aso, A. Hayashi and M. Tatsumisago, *Inorg. Chem.*, 2011, **50**, 10820–10824.